ELSEVIER

Contents lists available at ScienceDirect

Additive Manufacturing Letters

journal homepage: www.elsevier.com/locate/addlet



Short Communication

Additive manufacturing of recyclable, highly conductive, and structurally robust graphite structures



Mohammad Moein Mohammadi, Samuel Choi, Pratik Koirala, Gehan C. Jayatilaka, Neda Ghousifam, Hugo Celio, Mehran Tehrani*

Walker Department of Mechanical Engineering, The University of Texas at Austin, USA

ARTICLE INFO

Keywords: Graphite Additive manufacturing Cellulose Direct ink write Sustainability Recyclable Low energy

ABSTRACT

This study investigates the design and use of a printable, sustainable, aqueous paste for room-temperature low-energy material extrusion (ME) additive manufacturing (AM) of complex structures. To this end, pastes with controlled rheology and a total solid content of ~42% are formulated. Constituents of the pastes are commercial graphite and cellulose nanocrystal (CNC) powder, as a dispersing additive, with 91:09 and 88:12 graphite:cellulose wt.% compositions. The AM structures are dried in air at three rates (slow, medium, and fast). The structure of printed parts is characterized using electron microscopy, X-ray diffraction, Infrared/X-ray photoelectron spectroscopy, X-ray micro-computed tomography, and thermogravimetric analysis. The compressive strength of AM graphite structures reached 5.8±0.6 MPa with almost no effect from drying rates. However, samples containing more cellulose were ~30% stronger in compression. Carbonization of the AM parts increased their electrical conductivity by more than an order of magnitude to ~2400 S.m⁻¹. In addition, it enabled the fabrication of nearly pure graphite structures. The mechanical and electrical properties of samples fabricated in this study exceed the performance of previously reported AM graphite structures. Moreover, the recyclability of the printed parts was demonstrated by regenerating pastes via mixing printed parts in water and re-printing new parts with the paste. The AM graphite structures can be used in numerous applications, including but not limited to electrical discharge machining (EDM), electrochemical machining (ECM), high-temperature customized sealing, high-temperature composite tooling, and energy conversion and storage.

1. Introduction

Additive manufacturing (AM) offers high geometrical freedom and results in less waste than traditional methods [1–3]. Over the last few years, there has been a growing interest in making AM a more sustainable manufacturing technique [4]. Designing energy-efficient processes and environmentally friendly and recyclable materials are needed for AM's sustainable growth [5].

Currently, the most widely used AM techniques, such as selective laser sintering (SLS) and fused filament fabrication (FFF), require extensive amounts of energy to sinter powders or melt polymers [6]. Among various types of AM technologies focusing on minimizing energy consumption direct ink write (DIW) offers materials selection flexibility and potentially energy-efficient processing [7]. The challenges related to the DIW include developing inks that can be extruded and form self-supporting structures [8]. Thus, designing inks with specific rheological behaviors and finite yield stress is needed for DIW [9].

Research on sustainable material selection, preparation, and recycling is also essential for developing future AM techniques [3]. At

present, non-metallic materials used for AM are mainly based on non-biodegradable or petroleum-based polymeric materials [10]. In addition, wastes are produced due to failed prints or support structures that hold parts. Therefore, there is a trend in using biodegradable polymers and recycling AM polymeric parts. However, the main limitations in using such polymers are energy-intensive recycling processes and degradation of mechanical properties after recycling [11].

In recent years, as an alternative to polymers, eco-friendly, easily-accessible, and low-cost materials have been utilized for AM. As the most-abundant natural biopolymers, Cellulosic materials have emerged as suitable candidates for sustainable AM [12]. Cellulose nanomaterials (fibers or crystals) with unique properties such as high tensile strength and elastic modulus (130-150 GPa) and low density (~1.5 g.cm⁻³) have also been used as reinforcing fillers in different polymers [13]. More recently, cellulose-based materials have been used as AM's main component (not filler) [1]. Studies on the AM of cellulose nanocrystal (CNC) [7,14-16] and nanofibrillated cellulose (NFC) [17–19] demonstrate their potential for different applications. However, their primary challenge is retaining the shape of structures after printing. Because of the high

E-mail address: tehrani@utexas.edu (M. Tehrani).

^{*} Corresponding author.

water content in cellulose-based slurries (inks), their printed parts undergo drastic volumetric shrinkage upon drying [16]. Ideas to overcome this issue include one or a combination of the following: lyophilization (freeze-drying) after printing, which itself is an energy-intensive process and results in mechanically weak structures [20]; *in-situ* polymerization to prevent shrinkage, which makes the process not sustainable anymore [17,21]; and novel solvent-exchange [1], ionic cross-linking [18] or freeze-thawing [17] methods which only reduce shrinkage to some extent.

Graphite is another low-cost, earth-abundant carbon source with unique thermal and electrical properties [22] that is also gaining attention in the AM community as a sustainable material. Although there are reports for graphite's use as an additive for the AM of functional polymeric composites [23], research on the AM of graphitic structures has emerged recently. One example is creating 3D structures using a graphite-nanoclay paste [24], reporting a compressive strength and electrical conductivity of ~3.2 MPa and 555 S.m⁻¹, respectively, for their room-temperature dried 3D-printed parts. In another study, high-porosity, 3D aerogels of graphite-NFC are reported [25]. This study uses freeze-drying post-treatment to remove water and preserve the shape of the 3D-printed parts. Therefore, the reported compressive strength was as low as 0.5 MPa.

This paper aims to introduce a new class of sustainable and printable graphite pastes with tunable properties for additive manufacturing of prototypes and end-use parts without the need for any post-processing step. CNC is used as a rheology modifier and for dispersing low-cost commercial graphite powders in water. Specimens are printed using homogenous graphite-CNC pastes using a DIW printer at room temperature. The changes in porosity (void content), compressive strength, shrinkage, and electrical conductivity with respect to various compositions, drying rates, and carbonization are investigated.

2. Experimental section

2.1. Materials

Natural graphite (<45 μ m, \geq 99.99% trace metals basis) and cellulose nanocrystal (CNC) powders were acquired from Millipore Sigma (USA), and CelluForce Inc. (Canada), respectively. Deionized (DI) water was used in all experiments.

2.2. Slurry (ink) preparation

First, a certain amount of CNC powder was slowly added to DI water during mixing to make 6 or 8 wt.% dispersions. For all experiments, an IKA overhead shear mixer and a four-bladed propeller rotating at 2500 rpm were used to homogenize the dispersions. Graphite powders were then slowly added to the CNC dispersions followed by vigorous mixing to obtain ~42 wt.% total solid content homogenous pastes. Compositions of prepared pastes were approximately 91:09% graphite:CNC (G:C 91%) and 88:12% (G:C 88%) for the starting 6 and 8 wt.% CNC dispersions, respectively. To remove the trapped air bubbles, prepared pastes were centrifuged for 10 min at 3000 rpm using a Thermo Scientific SorvallTM ST 16 refrigerated centrifuge.

2.3. Additive manufacturing

Parts were fabricated using a retrofitted commercial 3D printer (Cura Lolzbot). Instead of the printer's nozzle head, an air-powered fluid dispenser (JB1113N, Fisnar) was mounted to control the paste flow rate. The overhead pressure for extrusion was 0.8-1.2 bar depending on the paste composition. The nozzle size was 0.84 mm (Gauge 18, SmoothFlow $^{\rm TM}$ tapered tip, Nordson EFD), and G-codes were generated using Cura Lolzbot slicing software with a printing speed of 20 mm.s $^{-1}$ and a layer height of 0.8 mm. After printing, parts were

dried under three different conditions: fast drying (FD), medium drying (MD), and slow drying (SD). For FD, the as-printed samples were kept under a fume hood at room temperature (\sim 21°C) for three days. For MD, samples were dried at room temperature (relative humidity of 65%) for three days, and for SD, samples were dried at a controlled humidity of 80-90% for 14 days. To ensure the complete removal of water, the dried samples were kept in a vacuum oven at 60°C overnight.

2.4. Material characterizations

Rheological properties of pastes were measured using a Discovery Series Hybrid Rheometer (DHR), model HR-2 from the TA Instruments, with a 40 mm parallel plate geometry, a gap of 0.5 mm, and a constant temperature of 23°C. Before starting each experiment, samples were kept at zero normal force without applying any pre-shear for 3 mins. Steady-state shear viscosity values were measured from 0.01 to 100 s⁻¹ with 5 points per decade. The storage (G') and loss (G") moduli were measured using an oscillatory logarithmical stress sweep at 1 Hz, and the yield strength was obtained from the intersection of the two. The crystal structures of graphite, CNC, and the printed part (G:C 91%) were determined by X-ray diffraction (XRD) analysis (Rigaku ULTIMA IV Diffractometer). The d-spacing of graphite-containing samples was estimated by the Debye-Scherrer equation based on the C (002) peak of the XRD patterns. Thermogravimetric analysis (Mettler Thermogravimetric Analyzer, Model TGA/DSC 1) was conducted in N2 from room temperature to 500°C at a heating rate of 10°C min⁻¹. The morphology of samples was examined using an environmental scanning electron microscopy (ESEM) instrument (FEI Quanta 650). Samples were sputter-coated with a thin layer of gold prior to characterization. To detect the surface functional groups of graphite, CNC, and the printed parts, Fourier transform infrared (FTIR) spectroscopy was conducted from 500 to 4000 cm⁻¹ using a Thermo Mattson spectrometer. XPS spectra were recorded using a commercial X-ray photoelectron spectrometer (Kratos Axis Ultra DLD, Manchester, U.K.), with a monochromated Al-Ka X-ray source ($h\nu = 1486.5$ eV), hybrid optics (employing a magnetic and electrostatic lens simultaneously) and a multi-channel plate coupled to a hemispherical photoelectron kinetic analyzer. The base pressure in the analysis chamber was $\sim 5 \times 10^{-9}$ Torr. The spectrometer was calibrated using the Cu 2p 3/2, Ag 3d 5/3, and Au 4f 7/2 peaks. Surveys were measured with a pass energy of 160, while high-resolution peaks were collected with a pass energy of 20 eV at 0.1 eV per step and four sweeps. All peaks were calibrated with respect to the graphite C1s at 284.3 eV. The charge neutralizer was used only for the cellulose sample. Casa XPS analysis software (v2.3.22, Casa Software Ltd, UK) was used for peak analysis and to determine the stoichiometry of samples. X-ray micro-computed tomography (μ CT) of 3Dprinted samples (G:C 91% dried at room temperature and G:C 88% dried at three different conditions) was obtained using an Xradia microXCT at UTCT, the University of Texas at Austin. High resolution (1 μ m/pixel) volumetric images covering a 2 mm cube were acquired for analysis. Dragonfly 4.0 was used to visualize the microstructure of each

2.5. Electrical and mechanical properties

Uniaxial compression tests in the build direction (z-direction) were conducted at room temperature using an MTS Electromechanical testing system with a 1 KN load cell and a constant crosshead displacement of 1 mm s $^{-1}$. Four printed cylinders of 12.7 mm in diameter and 25.4 mm in height were tested for each condition. The electrical conductivity of 3D-printed parts in the x-y direction was measured using the van der Pauw method. Coupons printed in cubes of $10\times10\times2$ mm³ were tested with a custom-made four-probe apparatus. The current was supplied by a Keithley 6221 DC/AC current source, and the voltage drop across the samples was measured by a Keithley 2182A Nanovoltmeter. To observe

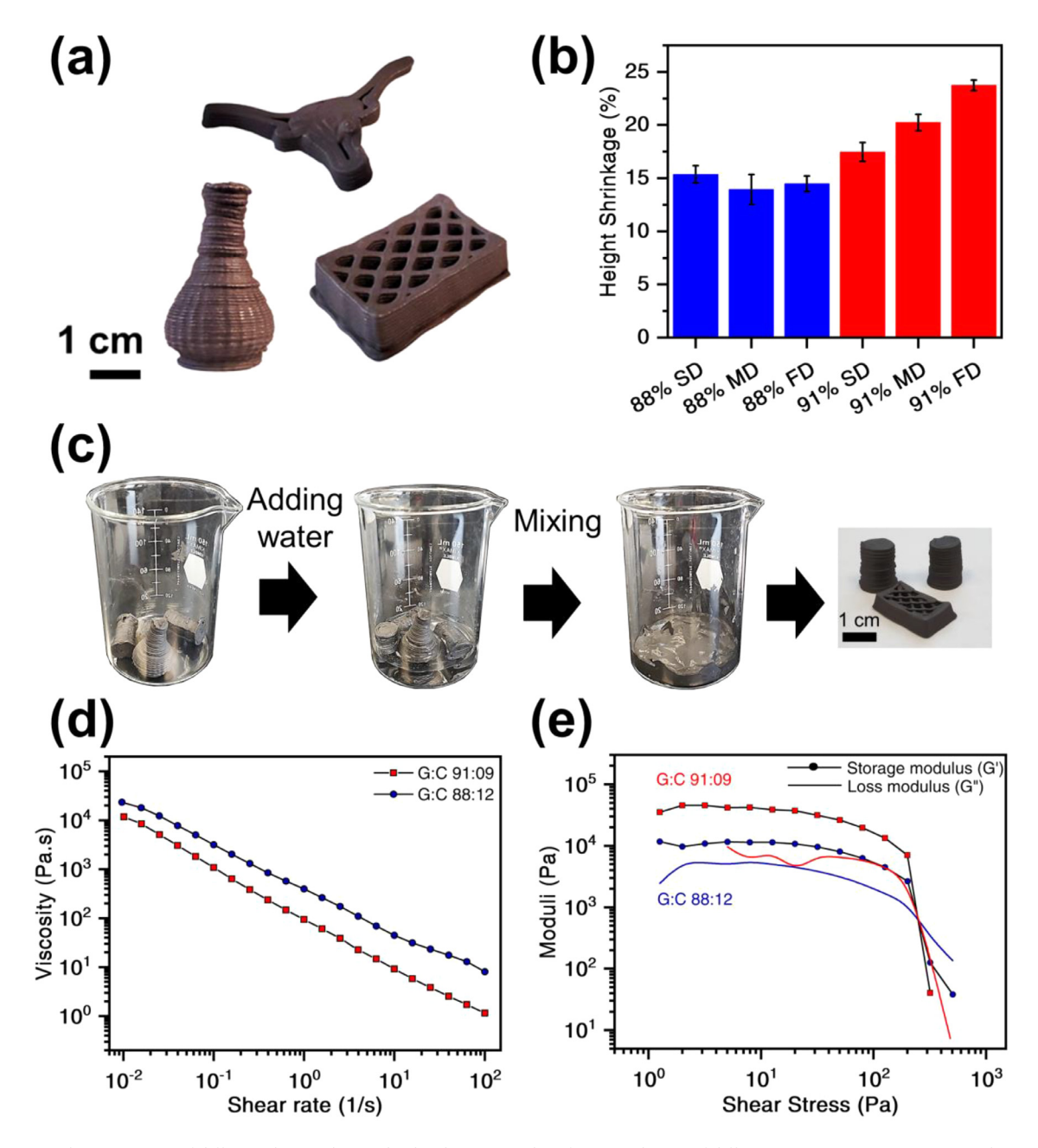


Fig. 1. (a) AM graphite structures of different shapes; (b) Height shrinkage (%) values for printed parts of different compositions (G:C 91:09 and G:C 88:12 wt.%) and different drying conditions (slow, medium, and fast drying: SD, MD, and FD); (c) Steps involved in the recyclability test of printed parts; (d, e) Rheological properties of the prepared pastes at two compositions confirming their shear-thinning behavior and printability (graphite:CNC or G:C of 88:12 and 91:09 wt.%).

the change in conductivity after CNC removal, samples were carbonized under $\rm N_2$ for 1 h at 400°C with a heating rate of 10°C $\rm min^{-1}$.

3. Results and discussion

Fig. 1a displays three additively manufactured structures made of graphite-cellulose (G-C). Parts were manufactured with a relatively high resolution using a 0.84 mm tapered nozzle (as compared with 1.54 mm [24] and 1 mm [25] nozzle sizes for the other two graphite additive manufacturing studies). The AM of these complex structures with curvatures and varying sizes confirms the capability of this technique for making geometries that cannot be readily manufactured by other conventional molding methods. Height shrinkage (%) for the AM cylinders of different compositions and drying conditions is compared in Fig. 1b. Although for all samples the radial shrinkage was negligible (less than 1%), the height

shrinkage was at least 12%. Such shrinkage could be attributed to the evaporation of the water in pastes (~58 wt.% or >70% vol.%). However, compared with the shrinkage numbers reported for other AM cellulose-based structures, these numbers are extremely lower. For instance, Jiang et al. reported ~40-50% height shrinkage for their freeze-dried cellulose honeycombs [19]. Françon et al. eliminated the freeze-drying step by developing a freezing-thawing-solvent exchange method, and printed structures with linear shrinkage of at least 30% [17]. Height shrinkage of 36% was reported for air-dried AM cellulose structures [26]. At the same total solid content, the pastes containing more cellulose resulted in structures with less shrinkage as observed elsewhere [18]. There was not a statistically noticeable difference in shrinkage values for the G:C 88:12 wt.% samples dried at different conditions. However, shrinkage increased for faster drying rates for the G:C 91:09 wt.% samples. Given that the samples mostly shrink in one direction, dimensionally accurate

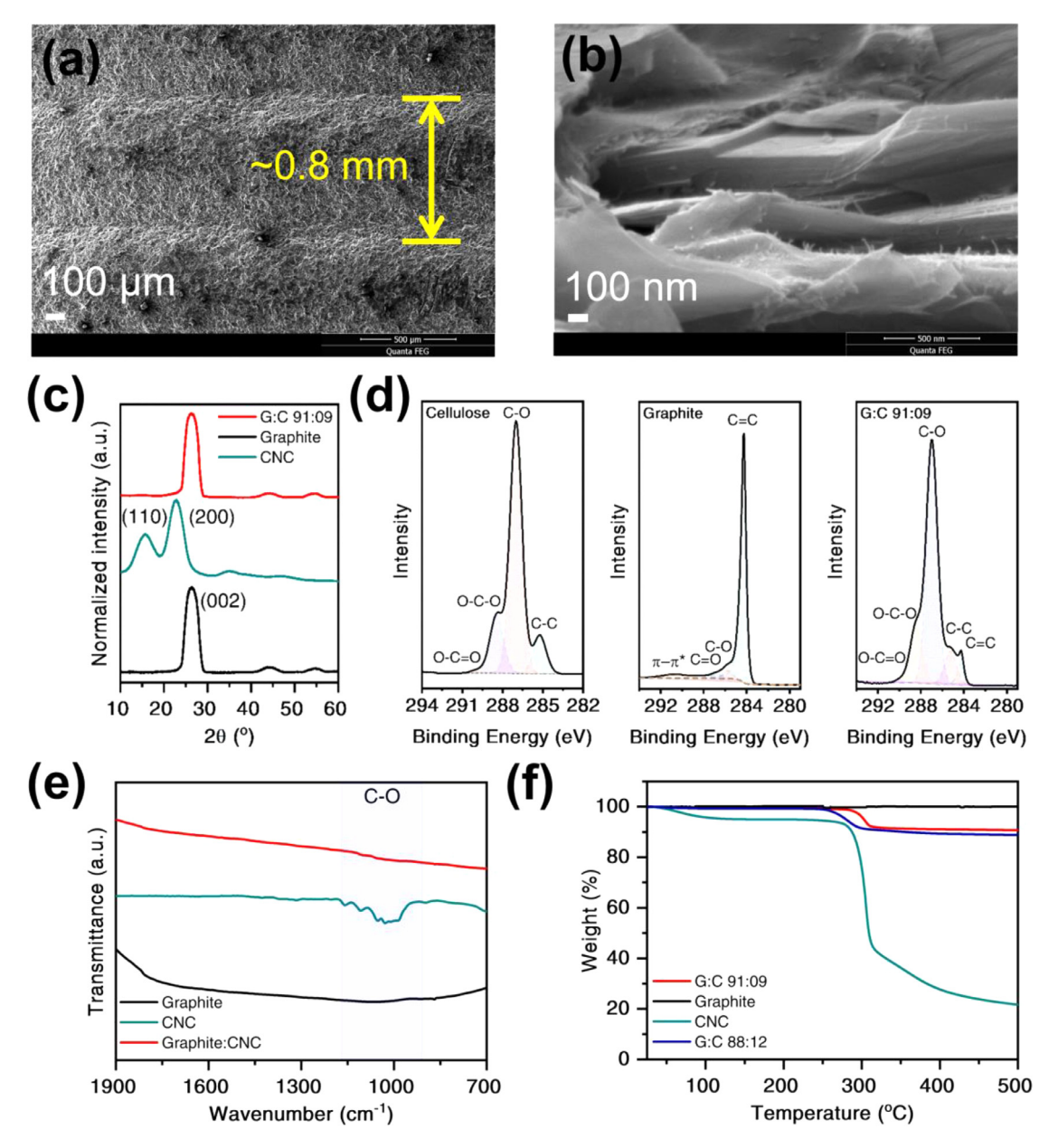


Fig. 2. SEM images of (a) side of a printed part, (b) Fractured surface of the composite sample consisting of graphite sheets and cellulose nanocrystals; (c) XRD patterns of graphite, CNC, and printed part (G:C 91:09 wt%); (d) XPS C 1s spectra of graphite, CNC, and dried filament; (e) FTIR spectra of graphite, CNC, and graphite:CNC; (f) Weight loss under nitrogen up to 500°C for graphite, CNC, and composite G-C at two compositions (91:09 and 88:12 wt%).

prints can be achieved by accounting for their shrinkage in the design stage.

Pastes with 42% solid content, the maximum concentration that could be prepared and printed with the current setup, were formulated. According to the screening experiments, at least 9% CNC is needed for making uniform pastes and preventing particle separation from water. For pastes containing less than 9% cellulose, two phases (particle-rich and water-rich) were observed after the degassing centrifugation step. On the other hand, due to the governing role of CNC on the overall viscosity, at most 12% CNC could be used. Adding more than 12% CNC to achieve a total solid content of 42% resulted in pastees that were not pumpable because of their extremely high viscosity. Fig. 1c demonstrates the recyclability of AM graphite structures. G-C structures are recycled by simply adding water to the dried printed parts followed by mixing to obtain a uniform paste and eventually re-printing. To evaluate the printability of the pastes, a series of rheological tests were con-

ducted. Fig. 1d shows the shear-thinning behavior of the prepared pastes at two different compositions. The pastes had high viscosities at low shear rates (above 10^4 Pa s at 0.01 s⁻¹) and experienced more than three orders of magnitude reduction in viscosity under shear rates usually applied in direct ink writing ($\sim 50 \text{ s}^{-1}$) [27]. This behavior corresponds to the presence of CNC in pastes and enables paste flow through narrow nozzles [28]. The higher viscosity of the paste with more CNC can be attributed to the stronger hydrogen bonding network structures formed among the chains of dissolved cellulose in the water [29]. Oscillatory logarithmical stress sweep measurements for both paste formulations are shown in Fig. 1e. A printable paste should possess several properties. First, while high solid contents are desirable to minimize shrinkage during drying, the paste should not contain any agglomerates. The maximum G-C content to achieve such paste was determined to be ~42%. Second, the paste should be pumpable, i.e., its viscosity should be low enough for the pump to deliver it from its container to the nozzle. Fi-

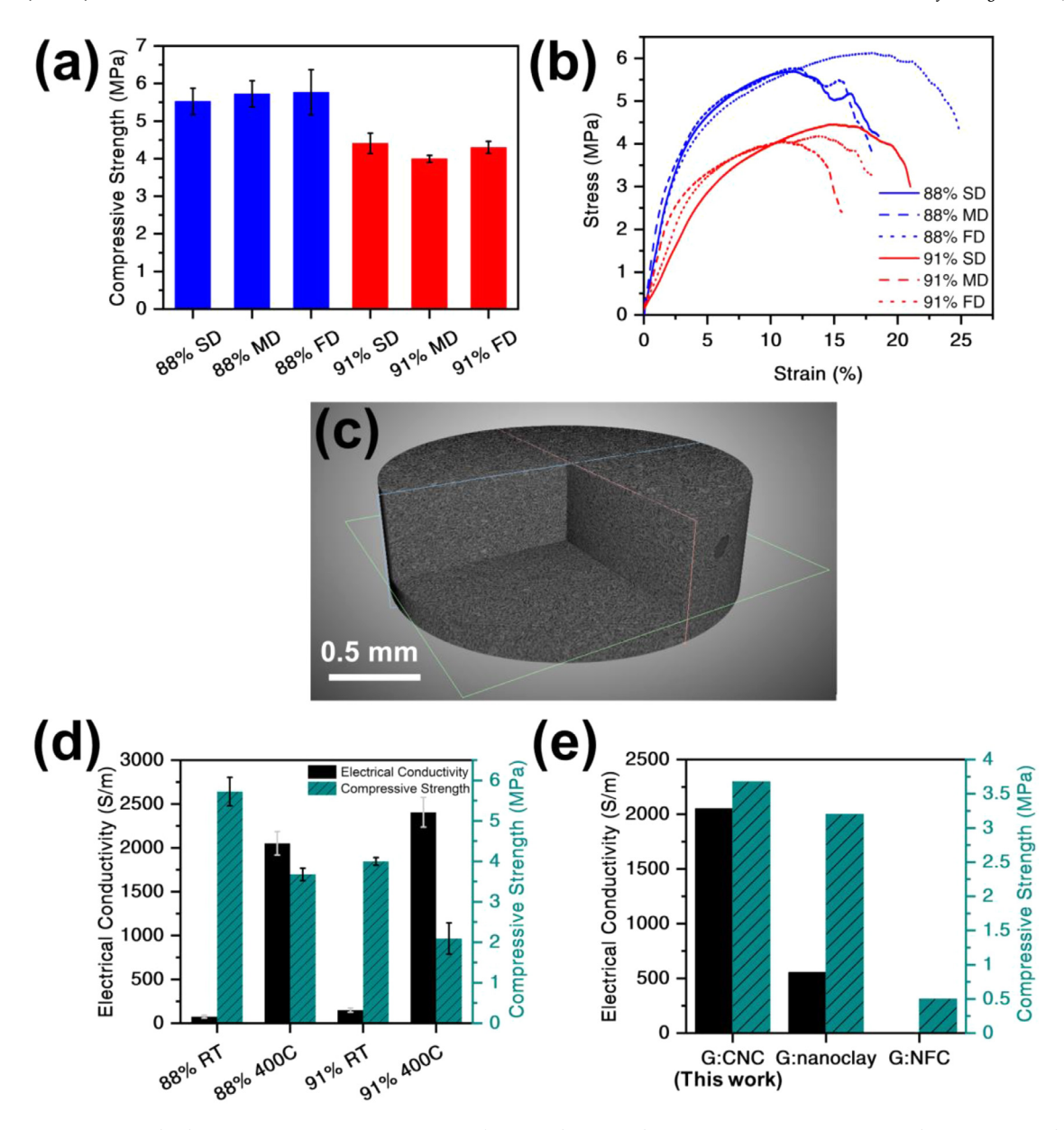


Fig. 3. (a) Compressive strength, (b) representative stress-strain curves for printed parts with two compositions (G:C 88:12 and 91:09 wt%) and three drying conditions (slow, medium, fast drying, SD-MD-FD); (c) a μCT image of the AM G:C (88% MD) structure (dark: void, gray: graphite); (d) Electrical conductivity and the corresponding compressive strength for as-prepared and carbonized printed parts; (e) Comparison of this work with the other two AM graphite structure studies: graphite:nanoclay [24], and graphite:nanofibrillated cellulose [25].

nally, it should achieve a high enough yield strength to retain its shape after deposition and under the weight of layers added on top of it. The last two criteria are usually opposing, i.e., rheology modifiers that enhance paste's yield strength also raise its viscosity. Based on these criteria, the G-C pastes were formulated to have 42% total solid content and shear yield strengths of 0.1-1 KPa. The pastes showed elastic behavior at low shear stresses (G' > G''), with the storage modulus being almost one order of magnitude larger than the loss modulus. Moreover, a large shear yield strength (when G' = G'') for both pastes (>200 Pa) confirms filament formation during printing and preserving the shape after printing [18].

Fig. 2a shows a side view SEM image of an AM graphite structure with visible ~ 0.8 mm thick layers. Fig. 2b displays a high-magnification SEM image of a fractured surface with layered graphite sheets and small rod-like cellulose nanocrystals on their surface. XRD patterns of graphite, CNC, and a printed G-C (91% graphite) structure are shown in Fig. 2c. Graphite has a major peak at $\sim 26.37^{\circ}$, corresponding to C

(002) plane [30]. For the CNC, the two characteristic peaks are at \sim 15.6° (broad) and \sim 22.8°, corresponding to (110) and (200) planes, respectively [31]. For the composite G-C, the pattern is more similar to that of graphite with the calculated d-spacing of 0.33 nm, suggesting no change in crystallinity upon mixing/printing.

Fig. 2 d displays XPS spectra for the C 1s region of CNC, graphite, and a dried extruded filament with a composition of G:C 91:09 wt.%. The C 1s spectrum of cellulose can be decoupled into four bonds, corresponding to C-C (285.2 eV), C-O (287.0 eV), O-C-O (288.4 eV), and O-C=O (~290.0 eV), respectively [32]. For graphite, it can be deconvoluted into C=C (284.3 eV), C-O (285.9 eV), C=O (287.9 eV), and π - π * (~290.7 eV), respectively [33]. Although the filament is graphite-rich, its XPS spectrum mostly shows cellulose-related bonds, suggesting the formation of a nanosized thin layer of cellulose on the surface of the filament. The spectrum contains C=C (284.3 eV) from graphite and C-C (285.3 eV), C-O (287.0 eV), O-C-O (288.4 eV), and O-C=O (~290.0 eV) from cellulose. Interestingly, a similar spectrum was observed for the

filament dried by a lyophilizer, suggesting the formation of such a CNC thin layer regardless of how it has been dried. FTIR spectra of graphite, CNC, and G:C (91% graphite) structures are shown in Fig. 2e. A series of peaks in the range of 900-1200 cm⁻¹ are present in the CNC spectrum that could be attributed to C-O stretching. Such peaks are absent in the spectrum of the G-C composite, probably due to the much higher concentration of graphite with respect to cellulose in the IR penetration depth of the sample. As shown in the TGA (Fig. 2f), cellulose-containing samples start degrading from ~270-300°C under a nitrogen environment, consistent with the thermal degradation of cellulosic materials [34]. For CNC powders, there is a slight decrease in mass at temperatures below 100°C, potentially due to the evaporation of adsorbed water molecules and hydroxyl groups. The residual mass (carbonized cellulose) reaches ~20% after reaching 500°C. For AM G-C structures, the total weight loss is attributed to the cellulose content (~10%), as graphite does not degrade when heated under an inert environment.

Fig. 3a and b show compressive strengths and representative stress-strain curves for AM G-C structures at different compositions and drying conditions. Measured compressive strengths vary from 4 to 6 MPa with almost negligible dependence on the drying condition (because the average values are within the uncertainty levels for each drying condition). The 88% graphite samples show more than 30% higher compressive strength compared with the 91% graphite ones. Cellulose chains interact with graphite sheets through their hydrophobic and hydrophilic sites: C-H groups interact with the hydrophobic plane of graphite sheets while the hydroxyl groups form hydrogen bonds with the defective edges of graphite sheets. Larger compressive strength values for cellulose-rich samples could be related to the strong network of hydrogen bonds between the rich hydroxyl groups along neighboring cellulose molecular chains [35].

A representative µCT image of the AM G-C (88% MD) structure is shown in Fig. 3c. The uniform combination of dark regions (air) and gray regions (graphite) confirms the high porosity of the printed structures. The minimum porosity that could be calculated from the corresponding two-dimensional tomographs was in the range of 39-42%. For 88% graphite structures, porosity values were closer to the lower end of the range, while for 91% graphite structures, the porosity was closer to 42%. This could be another reason for the higher compressive strength of cellulose-rich samples. The calculated density for the AM structures was in the range of 0.8-0.9 g cm⁻³, which results in larger porosity values for the samples (considering the density of graphite and cellulose to be ~2.2 and 1.5 g cm⁻³, respectively). However, as mentioned earlier, porosities calculated from the µCT analysis were based on micron-size pores that could be detected by the device. The µCT tomographs in two perpendicular planes (Fig. 3e) suggest that the structure of the printed parts is transversely isotropic. This is, however, not confirmed by conducting mechanical or electrical tests in different directions. As such, the reported electrical conductivities are measured in the printing plane and compressive strengths are along the build direction.

Electrical conductivities of as-prepared and carbonized AM structures are displayed in Fig. 3 d. Air-dried AM structures show a relatively low electrical conductivity (<200 S.m⁻¹) due to the higher percentage of cellulose, which is insulating. However, after carbonizing the samples at 400°C in an inert environment, samples became more conductive (>2000 S.m⁻¹) while maintaining their overall structural integrity. Using this carbonization technique, the electrical conductivity of the 88% G:C samples increased by an order of magnitude while their compressive strength decreased by only 30%. Moreover, such cellulose removal technique is suggested when printed parts are intended for use in high humidity or harsh environments. Finally, the electrical conductivity and compressive strength of the samples produced in this work are compared with the other two AM graphite structures reported recently (Fig. 3e). The compressive strengths of both as-prepared and carbonized G-C structures are larger than those reported by other groups. Moreover, the electrical conductivity of the as-prepared AM structure is in the same order of magnitude as the graphite:nanoclay printed parts and ${\sim}4$ times larger when carbonized.

4. Conclusions

In this study, conductive and strong additively manufactured structures were realized using printable, sustainable, and recyclable materials. Graphite, with unique electrical, thermal, and mechanical properties, was chosen as a low-cost abundant crystalline form of carbon. CNC powders were used to enable dispersion of graphite sheets in water and guaranteed printability of the prepared pastes. Using optimized pastes and the direct ink write AM technique, samples with complex geometries were manufactured at room temperature. Recyclability of the process was demonstrated by re-dispersing printed parts in water and reprinting with the paste. Rheological tests confirmed the shear-thinning and printability of the pastes. Bulk characterization techniques such as XRD showed peaks corresponding to graphite with no change in crystallinity during mixing and printing. XPS spectra confirmed the presence of a thin cellulose layer on graphite sheets, supposedly responsible for their homogenous dispersion in water. A deeper depth surface characterization technique, FTIR here, demonstrated the absence of main peaks related to cellulose. Although drying rate did not affect the mechanical properties significantly, paste composition did. The use of pastes with more cellulose resulted in AM structures with ~30% higher compressive strength (5.8±0.6 MPa). As confirmed by the TGA, most of the cellulose was carbonized at 400°C, resulting in highly conductive parts (~2400 S.m⁻¹). The compressive strength and electrical conductivity of samples measured in the present study exceed those of previously reported AM graphite structures.

Declaration of Competing Interest

The authors declare that they have no known competing financial interests or personal relationships that could have appeared to influence the work reported in this paper.

Acknowledgment

The authors acknowledge the support of the National Science Foundation (NSF) CAREER Award #2015732. The X-ray CT studies were conducted at the UTCT facility at the University of Texas at Austin.

References

- [1] K.M.O. Håkansson, I.C. Henriksson, C. de la Peña Vázquez, V. Kuzmenko, K. Markstedt, P. Enoksson, P. Gatenholm, Solidification of 3D Printed Nanofibril Hydrogels into Functional 3D Cellulose Structures, Adv. Mater. Technol. 1 (7) (2016).
- [2] B. Jiang, Y. Yao, Z. Liang, J. Gao, G. Chen, Q. Xia, R. Mi, M. Jiao, X. Wang, L. Hu, Lignin-Based Direct Ink Printed Structural Scaffolds, Small 16 (31) (2020) e1907212.
- [3] T. Peng, K. Kellens, R. Tang, C. Chen, G. Chen, Sustainability of additive manufacturing: an overview on its energy demand and environmental impact, Addit. Manuf. 21 (2018) 694–704.
- [4] J. Jiang, Y.-F. Fu, A short survey of sustainable material extrusion additive manufacturing, Aust. J. Mech. Eng. (2020) 1–10.
- [5] F.L. Bourhis, O. Kerbrat, J.-Y. Hascoet, P. Mognol, Sustainable manufacturing: evaluation and modeling of environmental impacts in additive manufacturing, Int. J. Adv. Manuf. Technol. 69 (9) (2013) 1927–1939.
- [6] S. Kumar, A. Czekanski, Roadmap to sustainable plastic additive manufacturing, Mater. Today Commun. 15 (2018) 109–113.
- [7] G. Siqueira, D. Kokkinis, R. Libanori, M.K. Hausmann, A.S. Gladman, A. Neels, P. Tingaut, T. Zimmermann, J.A. Lewis, A.R. Studart, Cellulose Nanocrystal Inks for 3D Printing of Textured Cellular Architectures, Adv. Funct. Mater. 27 (12) (2017).
- [8] O. Uitz, P. Koirala, M. Tehrani, C.C. Seepersad, Fast, low-energy additive manufacturing of isotropic parts via reactive extrusion, Addit. Manuf. 41 (2021) 101919.
- [9] A. M'Barki, L. Bocquet, A. Stevenson, Linking Rheology and Printability for Dense and Strong Ceramics by Direct Ink Writing, Sci. Rep. 7 (1) (2017) 6017.
- [10] X. Wang, M. Jiang, Z. Zhou, J. Gou, D. Hui, 3D printing of polymer matrix composites: a review and prospective, Compos. Part B 110 (2017) 442–458.
- [11] K. Mikula, D. Skrzypczak, G. Izydorczyk, J. Warchoł, K. Moustakas, K. Chojnacka, A. Witek-Krowiak, 3D printing filament as a second life of waste plastics—a review, Environ. Sci. Pollut. Res. 28 (10) (2021) 12321–12333.
- [12] L.Y. Ee, S.F. Yau Li, Recent advances in 3D printing of nanocellulose: structure, preparation, and application prospects, Nanoscale Adv. 3 (5) (2021) 1167–1208.

- [13] H. Du, W. Liu, M. Zhang, C. Si, X. Zhang, B. Li, Cellulose nanocrystals and cellulose nanofibrils based hydrogels for biomedical applications, Carbohydr. Polym. 209 (2019) 130–144.
- [14] M.K. Hausmann, P.A. Ruhs, G. Siqueira, J. Lauger, R. Libanori, T. Zimmermann, A.R. Studart, Dynamics of Cellulose Nanocrystal Alignment during 3D Printing, ACS Nano 12 (7) (2018) 6926–6937.
- [15] V.C. Li, C.K. Dunn, Z. Zhang, Y. Deng, H.J. Qi, Direct Ink Write (DIW) 3D Printed Cellulose Nanocrystal Aerogel Structures, Sci. Rep. 7 (1) (2017) 8018.
- [16] V. Klar, J. Pere, T. Turpeinen, P. Karki, H. Orelma, P. Kuosmanen, Shape fidelity and structure of 3D printed high consistency nanocellulose, Sci. Rep. 9 (1) (2019) 3822.
- [17] H. Françon, Z. Wang, A. Marais, K. Mystek, A. Piper, H. Granberg, A. Malti, P. Gaten-holm, P.A. Larsson, L. Wågberg, Ambient-Dried, 3D-Printable and Electrically Conducting Cellulose Nanofiber Aerogels by Inclusion of Functional Polymers, Adv. Funct. Mater. 30 (12) (2020).
- [18] Y. Chen, Z. Yu, Y. Ye, Y. Zhang, G. Li, F. Jiang, Superelastic, Hygroscopic, and Ionic Conducting Cellulose Nanofibril Monoliths by 3D Printing, ACS Nano 15 (1) (2021) 1869–1879.
- [19] J. Jiang, H. Oguzlu, F. Jiang, 3D printing of lightweight, super-strong yet flexible all-cellulose structure, Chem. Eng. J. 405 (2021).
- [20] V.C.F. Li, A. Mulyadi, C.K. Dunn, Y. Deng, H.J. Qi, Direct Ink Write 3D Printed Cellulose Nanofiber Aerogel Structures with Highly Deformable, Shape Recoverable, and Functionalizable Properties, ACS Sustain. Chem. Eng. 6 (2) (2018) 2011–2022.
- [21] M.K. Hausmann, G. Siqueira, R. Libanori, D. Kokkinis, A. Neels, T. Zimmermann, A.R. Studart, Complex-Shaped Cellulose Composites Made by Wet Densification of 3D Printed Scaffolds, Adv. Funct. Mater. 30 (4) (2019).
- [22] L. Li, D. Zhang, J. Deng, Y. Gou, J. Fang, H. Cui, Y. Zhao, M. Cao, Carbon-based materials for fast charging lithium-ion batteries, Carbon 183 (2021) 721–734.
- [23] R. Haney, P. Tran, E.B. Trigg, H. Koerner, T. Dickens, S. Ramakrishnan, Printability and performance of 3D conductive graphite structures, Addit. Manuf. 37 (2021) 101618
- [24] S.M. Sajadi, S. Enayat, L. Vásárhelyi, A. Alabastri, M. Lou, L.M. Sassi, A. Kutana, S. Bhowmick, C. Durante, Á. Kukovecz, A.B. Puthirath, Z. Kónya, R. Vajtai, P. Boul, C.S. Tiwary, M.M. Rahman, P.M. Ajayan, Three-dimensional printing of complex graphite structures, Carbon 181 (2021) 260–269.

- [25] D. Liu, C. Chen, Y. Zhou, Y. Bao, R. Wang, Y. Liu, S. He, H. Huang, C. Zhang, B. Foster, T. Li, L. Hu, 3D-Printed, High-Porosity, High-Strength Graphite Aerogel, Small Methods 5 (7) (2021) 2001188.
- [26] C. Thibaut, A. Denneulin, S. Rolland du Roscoat, D. Beneventi, L. Orgeas, D. Chaussy, A fibrous cellulose paste formulation to manufacture structural parts using 3D printing by extrusion, Carbohydr. Polym. 212 (2019) 119–128.
- [27] B.G. Compton, J.A. Lewis, 3D Printing: 3D-Printing of Lightweight Cellular Composites (Adv. Mater. 34/2014), Adv. Mater. 26 (34) (2014) 6043–6043.
- [28] L.A.E. Müller, T. Zimmermann, G. Nyström, I. Burgert, G. Siqueira, Mechanical Properties Tailoring of 3D Printed Photoresponsive Nanocellulose Composites, Adv. Funct. Mater. 30 (35) (2020).
- [29] O. Korhonen, T. Budtova, Gelation of cellulose-NaOH solutions in the presence of cellulose fibers, Carbohydr. Polym. 224 (2019) 115152.
- [30] M.M. Mohammadi, S. Shao, S. Srivatsa Gunturi, A.R. Raghavan, N. Alexander, Y. Liu, C.M. Stafford, R.D. Buchner, M.T. Swihart, A general approach to multicomponent metal-decorated crumpled reduced graphene oxide nanocomposites using a flame-based process, Nanoscale 11 (41) (2019) 19571–19578.
- [31] J. Gong, J. Li, J. Xu, Z. Xiang, L. Mo, Research on cellulose nanocrystals produced from cellulose sources with various polymorphs, RSC Adv. 7 (53) (2017) 33486–33493.
- [32] A. Alanis, J.H. Valdés, N.-V. María Guadalupe, R. Lopez, R. Mendoza, A.P. Mathew, R. Díaz de León, L. Valencia, Plasma surface-modification of cellulose nanocrystals: a green alternative towards mechanical reinforcement of ABS, RSC Adv. 9 (30) (2019) 17417–17424.
- [33] X. Chen, X. Wang, D. Fang, A review on C1s XPS-spectra for some kinds of carbon materials, Fullerenes, Nanotubes and Carbon Nanostructures 28(12) (2020) 1048-1058.
- [34] Q. Xie, S. Wang, X. Chen, Y. Zhou, H. Fang, X. Li, S. Cheng, Y. Ding, Thermal stability and crystallization behavior of cellulose nanocrystals and their poly(I-lactide) nanocomposites: effects of surface ionic group and poly(d-lactide) grafting, Cellulose 25 (12) (2018) 6847–6862.
- [35] Y. Zhou, C. Chen, S. Zhu, C. Sui, C. Wang, Y. Kuang, U. Ray, D. Liu, A. Brozena, U.H. Leiste, N. Quispe, H. Guo, A. Vellore, H.A. Bruck, A. Martini, B. Foster, J. Lou, T. Li, L. Hu, A printed, recyclable, ultra-strong, and ultra-tough graphite structural material, Mater. Today 30 (2019) 17–25.